Electrochimica Acta 326 (2019) 134989

Contents lists available at ScienceDirect

Electrochimica Acta

journal homepage: www.elsevier.com/locate/electacta

Interfacial behavior of water-in-salt electrolytes at porous electrodes and its effect on supercapacitor performance

Kiran Mahankali [a, 1], Naresh Kumar Thangavel [a, 1], Yi Ding [b], Susil K. Putatunda [c], Leela Mohana Reddy Arava [a, *]

[a] Department of Mechanical Engineering, Wayne State University, Detroit, MI, 48202, USA
[b] U.S. Army Tank Automotive Research Development & Engineering Center, Warren, MI, 48397, USA
[c] Department of Chemical Engineering and Material Science, Wayne State University, Detroit, MI, 48202, USA

ARTICLE INFO

Article history:
Received 24 June 2019
Received in revised form
24 September 2019
Accepted 30 September 2019
Available online 4 October 2019

Keywords:
Water-in-salt electrolyte
Interfacial behavior
In situ Raman
Pore size
Surface area
Supercapacitor performance

ABSTRACT

Though Water-in-salt (WIS) electrolytes offer a wide potential window for energy storage device operation in aqueous conditions that can deliver high energy density, their high viscosity and low ionic conductivity certainly limits the rate performance of the devices. Herein, we present electrical double layer behavior and nature of transportation of WIS ions at different porous electrode interfaces using in situ Raman spectroscopy and electrochemical impedance spectroscopy (EIS). The in situ Raman analysis shows that, in activated carbon electrodes (pore size > 30 nm), the WIS electrolyte ions diffuse into the pore network and charge/discharge potential dictates the ion dynamics at the interface. Whereas, these ions undergo adsorption phenomena on graphene electrodes (pore size < 3 nm), thus facilitating rapid sorption of ions during charge-discharge. EIS study presented herein, with detailed bode plot analysis elucidates the dependence of capacitance, rate capability of the supercapacitor on the nature of electrodes and their pore size. In a typical supercapacitor cell, graphene electrodes with WIS electrolyte delivered a very high specific energy of 55.3 Wh/kg at a specific power of 2.4 kW/kg, unparalleled to any of the existing WIS electrolyte reports. The current studies provide experimental insights into ion storage and their dynamic mechanism at the interface formed by WIS electrolytes that will assist in designing of suitable electrode materials.

© 2019 Elsevier Ltd. All rights reserved.

1. Introduction

Electrochemical double layer capacitors (EDLCs) are high power energy storage devices that stems from reversible adsorption/desorption of ions at the porous carbon surface [1–5]. Due to this simple ion storage mechanism, the so-called non-faradaic reaction, EDLCs can be fully charged/discharged within seconds which makes it attractive for devices that require quick power delivery or uptake [6]. However, their energy density (~10 Wh/kg) is lower than conventional lithium-ion batteries [7] and hence, the research trends focus on improving EDLC's energy density while preserving the power density skill for extensive applications. Given the ion adsorption dependence on capacitance, nanostructured porous carbons designed with high surface area and controlled pore sizes balance both the power and energy at certain levels [8]. On the other hand, widening the voltage window for the device is given the utmost priority, since the energy density is proportional to the voltage squared. Organic solvents, polymer, and ionic liquid-based electrolytes offer a broad voltage window; however, low boiling point and high viscosity of these electrolytes pose safety concerns and slow down the device performance metrics upon extended cycling [2,9–11].

Aqueous electrolytes have proven to be cost-efficient and provide better safety regulations in addition to their superior ionic conductivity and mass transport at the electrode/electrolyte interface [12–14]. However, water electrolysis at 1.23 V limits the energy density to the lowest levels and the water decomposition deteriorates the EDLC's performance. Often, this issue can be circumvented by adjusting the alkalinity or by using a high concentration of salts in water, so as to shift the water decomposition potential downwards allowing EDLC's operation in an extended voltage window [3–5]. These concerns led the research

* Corresponding author.
E-mail address: larava@wayne.edu (L.M.R. Arava).
[1] K.M and N.T contributed equally to this work.

https://doi.org/10.1016/j.electacta.2019.134989
0013-4686/© 2019 Elsevier Ltd. All rights reserved.

towards designing aqueous electrolytes that operate in a potentially high voltage window compared to any other above-mentioned solvents. Recently, the thermodynamic potential of water splitting reaction was pushed to above 3 V by adding a super concentration of salts in water, which resulted in the so-called "Water-in-salt (WIS)" electrolytes which have shed some light on wide potential window operation [15,16]. Such a high concentration of salt outnumbers the solvent by weight & volume which strongly deviates the ionic atmospheres at the interface and they start to overlap, resulting in a collapse or compression of the diffusion layers and redistribution of ions [17,18]. These unusual interfacial modifications with highly concentrated solutions and physiochemical transformations produce solid electrolyte interphase (SEI) layer on the electrode surface, similar to the non-aqueous/ionic liquid medium, that motivates the use of these WIS electrolytes for Li-ion battery applications [16,19,20].

Similarly, WIS electrolyte was employed in EDLC applications and drastic improvement in capacitance and energy density of the system were realized [21,22]. To improve the EDLC performance, several approaches including a variation of salt concentration and employment of monolithic mesoporous carbon were explored [23,24]. However, all the previous results revealed that the EDLC has shown limited power density metrics in WIS electrolytes which is certainly due to their low ionic conductivity. In this regard, more understanding concerning the electrochemical properties of the WIS electrolyte's interface is still very appealing and certainly needs more attention. The inter ion interactions of WIS electrolyte ions at the interface is in close resemblance with that of the electrode/ionic liquid circumstances and is well understood from the recent studies using molecular dynamics, galvanic charge/discharge studies, etc [25–30]. These studies provide experimental evidence for the changes occurring in the double-layer structure formed at the interface as a function of carbon pore networks in the ionic liquid electrolytes and explains ionic dynamics through that. Further, the observation of pore size and surface area effects have led to a wave of interest in the mechanism of charge storage in porous carbon electrodes which elucidates fundamental knowledge about the changes in charging rates especially in the case of concentrated electrolytes [31,32].

Such an understanding remains unknown in the WIS class of electrolytes and it is crucial to explore those areas in order to improve the performance of WIS electrolytes in energy storage applications. To understand the interfacial changes involved in WIS electrolyte with respect to pore size and surface area of different carbon structures (activated carbon, AC and graphene, Gr), we have performed systematic in situ Raman spectroscopy studies at the electrode/electrolyte interface using a specially designed liquid-immersion lens. The obtained results were further corroborated by electrochemical impedance spectroscopy (EIS). In addition, the effect of carbon structures/WIS electrolyte interface on energy and power density of supercapacitor (SC) was demonstrated with typical charge/discharge studies. Furthermore, the performance of WIS electrolyte in supercapacitor devices was effectively discussed with help of cycle life, Ragone plot and capacitance retention.

2. Experimental section

2.1. Materials

Lithium bis(trifluoromethanesulfonyl)imide (LiTFSI), N-Methyl-2-pyrrolidone (NMP), Polyvinylidene fluoride (PVDF) were obtained from Sigma Aldrich. Activated Carbon (AC, ~20–40 mesh) was procured from Alfa Aesar. Graphene (Gr) was obtained from Angstrom materials.

2.2. Carbon electrode modification and electrolyte preparation

AC and Gr activation was done using a process described elsewhere [33]. Briefly, AC and Gr materials were subjected to 1 M phosphoric acid (H_3PO_4) solution. The activation process was then carried out by heating the samples at a rate of 3 °C/min to 800 °C under argon gas flow. The samples were then held at activation temperature for 90 min under argon environment and was then cooled down to room temperature. The product was subsequently washed with deionized water and was finally oven-dried at 120 °C overnight under vacuum condition. The concentrated electroyte used for all the studies was prepared by dissolving 21 mol of LiTFSI salt in 1 kg of water solvent (denoted as 21 m), as described else where [15].

2.3. Characterization

The morphology and microstructure of the AC and Gr materials were characterized using field emission scanning electron microscopy (JSM-7600, FESEM). The surface area, pore diameter and pore size of AC and Gr were analyzed by recording Brunauer-Emmett-Teller (BET) nitrogen gas (N_2) absorption-desorption isotherms (BET, Micromeritics, Tristar II). The samples were degassed at 150 °C for 5 h to remove moisture and any other adsorbed gases from the surface. Then N_2 sorption isotherms were obtained at −196 °C using pure N_2 gas. Pores size distribution was analyzed using the BJH method from the desorption branch of the isotherms.

2.4. Electrode fabrication

The active materials (activated carbon and graphene), were mixed separately with PVDF and carbon black in a mass ratio of 80:10:10. Each composition was ground together with the NMP solvent for 2 h. After grinding the respective materials, the mixtures were blended thoroughly to obtain uniform slurries. These slurries were then coated on a carbon paper, that was used as a current collector and then dried in vacuum, overnight at 70 °C. Finally, after 12 h, electrodes with a uniform thickness of 0.1 mm were obtained.

2.5. Electrochemical measurements

Electrochemical impedance spectroscopy (EIS), cyclic voltammetry (CV) and galvanostatic charge-discharge (GCD) measurements were recorded using a potentiostatic/galvanostatic (Biologic, EC-Lab SP-200) in a two-electrode configuration. The two-electrode supercapacitor cells (represented as AC SC and Gr SC) were fabricated in a Swagelok type cell using two electrodes of identical mass sandwiched with a glass fiber separator. Prior to fabrication, the separator was wetted with 20 μl of the electrolyte. The specific capacitance (F/g) of the devices was calculated by the total mass of active materials alone (on both electrodes) that are used in the cell.

Imaginary (C") and real capacitances (C') from the bode plot are given by the following equations [34],

$$C'(\omega) = \frac{Z''(\omega)}{\omega |Z(\omega)|^2} \quad (1)$$

$$C''(\omega) = \frac{Z'(\omega)}{\omega |Z(\omega)|^2} \quad (2)$$

where, $|Z(\omega)|^2 = Z'(\omega)^2 + Z''(\omega)^2$ and $\omega = 2\pi f$, f is the AC frequency (Hz), Z' (ω) is the real impedance, Z" (ω) is the imaginary impedance.

The Device capacitance (C_m), specific capacitance (C_s), power density (P_s) and energy density (E_s) were calculated from the GCD measurements using the following equations [35–37]:

$$C_m = I/m\ (dV/dT)\ (F/g) \tag{3}$$

where, I is the applied current density (in A/g), dV/dt is calculated from the slope of the discharge curve, m is the mass of both electrodes.

$$C_s = 4{*}C_m\ (F/g) \tag{4}$$

$$P_s = \frac{V \times I}{M}(W/kg) \tag{5}$$

where, $V = \frac{V_{max}+V_{min}}{2}$, V_{max} and V_{min} are the maximum and minimum values of operating potential window, I is the current applied, M is the total active mass of both electrodes

$$E_s = Ps{*}\frac{t}{3600}(Wh/kg) \tag{6}$$

where, P_s is the power density, t is the discharge time.

2.6. In situ Raman spectroscopy cell setup

In situ Raman spectroscopy was performed using an in-house built three electrode electrochemical cell with 532 nm green laser (Nd-YaG) and CHI-760E bipotentiostat instrument. The Raman experiments were carried out with a liquid-immersion objective which decreases the refractive index mismatch between the electrode and electrolyte, thus improving the overall sensitivity and spatial resolution of the measurements. Here, activated carbon/graphene on carbon paper was used as working electrode and platinum, silver wires as counter and reference electrodes respectively. The working electrodes were prepared by pressing active material onto a carbon paper. A similar mass loading of both carbon materials was maintained (~1.0 mg) for the experiment. Typical Raman spectrum was recorded continuously, under chronopotentiometry conditions at a current density of 0.05 A/g, for every 10-mV change in the potential between −1.1 V and 1.5 V and presented herein. The band intensities used for the data analysis in this study were baseline corrected.

3. Results and discussion

To explore the dynamic behavior of LiTFSI ions at the interface, we performed in situ Raman spectroscopy experiments on SC electrodes. For this purpose, we have chosen two carbonaceous materials, a low surface area activated carbon and high surface area graphene. Previously, the SEM images and BET isotherm of AC, Gr electrodes were recorded and presented in Fig. S1 and Fig. S2 respectively. As shown in Fig. S2a, AC exhibits a combined characteristic of type I and type IV isotherm with a slight N_2 uptake ($P/P_o = 0-0.1$) and a hysteresis loop ($P/P_o = 0.5$ to 1.0) demonstrating the co-existence of mesopores and macropores [38,39]. On the other hand, as shown in Fig. S2c, the isotherm of Gr exhibits a type IV curve [40,41], with a clear hysteresis loop in the pressure region between 0.50 and 1.0, depicting a well-developed mesoporous structure. Further, Gr electrodes exhibited a sharp distinct rise in adsorption at P/P_o ~1, compared to AC, due to the limited uptake of N_2 depicting a capillary condensation phenomenon in the mesopores. In addition, the pore size distribution curves (Fig. S2 b, d) confirm the presence of a high-density of uniform mesopores at 2–3 nm for the Gr whereas, high volume of macropores (pore size > 30 nm) with limited mesopores were observed in AC electrodes. Further, the surface area of AC and Gr were found to be 277.34 m^2/g and 959.37 m^2/g respectively. The interfacial behavior of WIS electrolytes on the carbons with these porosities and surface areas was assessed and discussed in the following sections.

Fig. 1a shows representative Raman spectra of the WIS electrolyte/AC interface with respect to the applied potential. The

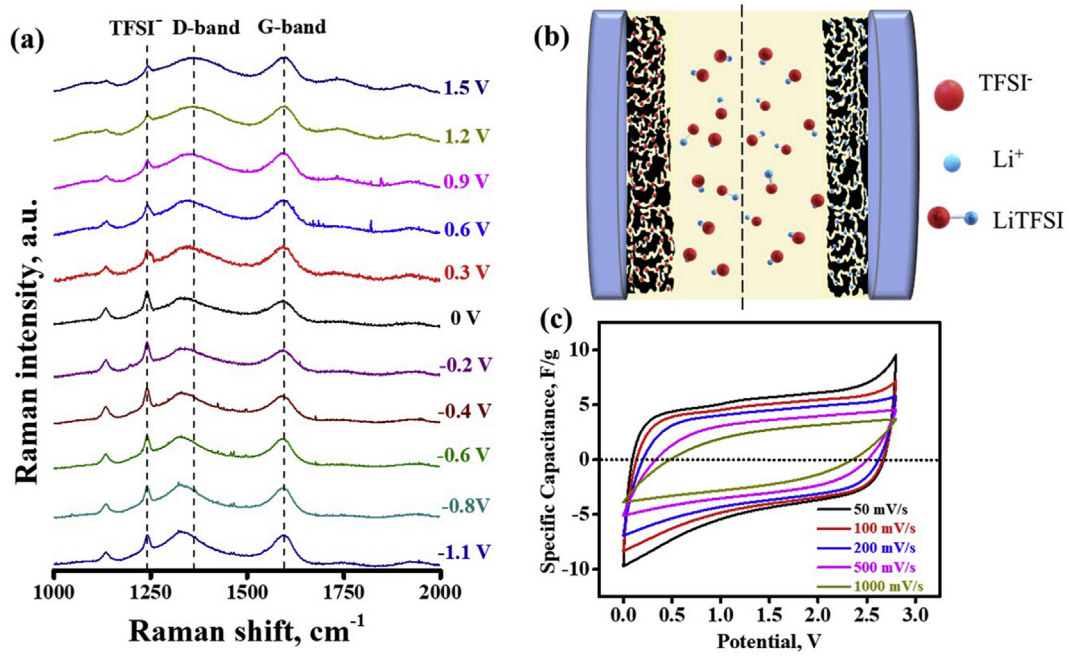

Fig. 1. Insitu Raman experiment at activated carbon SC electrodes: (a) LiTFSI anion and cation responses with respect to the applied potential (range from −1.1 V to 1.5 V) (b) Schematic illustration of diffusion of LiTFSI ions at highly porous AC SC electrodes (c) Cyclic voltammetric response of AC electrodes at different scan rates (range from 50 mV/s to 1000 mV/s).

Raman spectrum at open circuit potential shows vibrational bands of LiTFSI [42] (1135 – SO_2 symmetric stretching vibration, 1245 cm^{-1} - CF_3 symmetrical stretching vibration, 1316 cm^{-1} - SO_2 asymmetrical stretching vibration, 1575 cm^{-1} - C–C stretching) and typical carbon peaks [43,44] such as D-band (1350 cm^{-1}) and G-band (1585 cm^{-1}). Here, to understand the nature of WIS electrolyte ions transporting across the interface, change in Raman intensity of $TFSI^-$ anions with respect to positive and negative potential sweeps, under chronopotentiometry conditions (Fig. S3) was monitored. During the positive potential sweep (Fig. 1a), as the voltage increases from 0 to 1.5 V, the anionic molecule's Raman intensity linearly decreased with the applied potential. The fading of the Raman signal can be attributed to the LiTFSI ions entering the porous network, with increasing potential. While reversing the potential, anion intensity started to increase until a certain point (−0.4 V) which indicates the exiting of WIS ions from the carbon pores. On the other hand, similar to the results observed in a positive direction, at deep negative potential region (>−0.5 V) until −1.1 V, $TFSI^-$ anion Raman intensity started to decrease (Fig. 1a) which indicates the transportation of WIS ion again into the pores. This voltage dictated behavior can be explained by the heavily solvated, interionic interactive nature of ion-rich WIS interface and this phenomenon is well supported by previous reports including molecular dynamic studies [29,30]. These results reveal that, while charging and discharging, the LiTFSI ions tend to enter inside the porous carbon network. Also, due to the heavy solvation nature of WIS ions at the interface, instead of separation, the ion pairs (Li^+ $TFSI^-$) might diffuse into/expel from the pores as a cluster of molecules during charge/discharge process. Hence, from the Raman results it is clearly evidenced that ion rich LiTFSI ions diffuse into the porous AC carbon network (as shown schematic in Fig. 1b) and obviously AC contains a huge network of interconnected-wide size ranged pores with moderate surface area, which leads to the migration of the $TFSI^-$ ions deep into the porous structure, thereby limiting the rate capability especially during fast scan rates. Such behavior is further accounted for by cyclic voltammetry graphs, as shown in Fig. 1c, at symmetrical SC cell with AC and WIS as electrode and electrolyte respectively at different scan rates. Prior to CV, the potential window of WIS electrolyte was assessed and typical capacitance behavior, that is, rectangular shape of CV was observed until 2.9 V (Fig. S4 demonstrates the usefulness of these electrolytes for SC operation significantly above the thermodynamic stability (1.23 V) limit of aqueous electrolytes [45]). At lower scan rates, up to 200 mV/s, the cell exhibited a near rectangular behavior. But, as the scan rate increases above 200 mV/s, traditional supercapacitor electrodes (e.g., activated carbon) become less capacitive and more resistive, which is evident as the shape of the CV curves drastically deviates from the rectangular shape (Fig. S5 a, b). This behavior can be attributed to the dependence of double layer capacitance on the surface area, the pore size of the electrode and ionic size of the electrolyte, which was well established by previous results [31].

Fig. 2a shows the in situ Raman spectra of WIS electrolyte in a Gr electrode setup at different voltages during a potential sweep from −1.1 to +1.5 V (Fig. S6). The Raman spectra of LiTFSI in the electrodes in the charged state and discharged state remain the same. Furthermore, there is no shift in any Raman peak intensity during charge and discharge conditions, suggesting that the ion-rich environment does not change significantly with respect to the potential at the Gr interface. This is exactly opposite to the results obtained for the AC electrodes, where a predominant difference in the spectra of the charged and discharged conditions was observed. This Raman results can be ascribed to the WIS ions predominantly undergoing surface adsorption process, rather than diffusion into the pores, where they can still be detected by the Raman irrespective of the charge-discharge process; thus, only a small change can be expected. Fig. 2b illustrates the charging mechanism for graphene electrodes, where the $TFSI^-$ ions are adsorbed on the surface of graphene layers and obviously, during discharge, the adsorbed ions move away from the surface, without affecting the bulk of the electrolyte. Such availability of ions closes to the electrode surface and charge storage phenomenon occurring at the surface decreases the ion pathway distances thereby enhancing the high charge/discharge rates. In short, the high

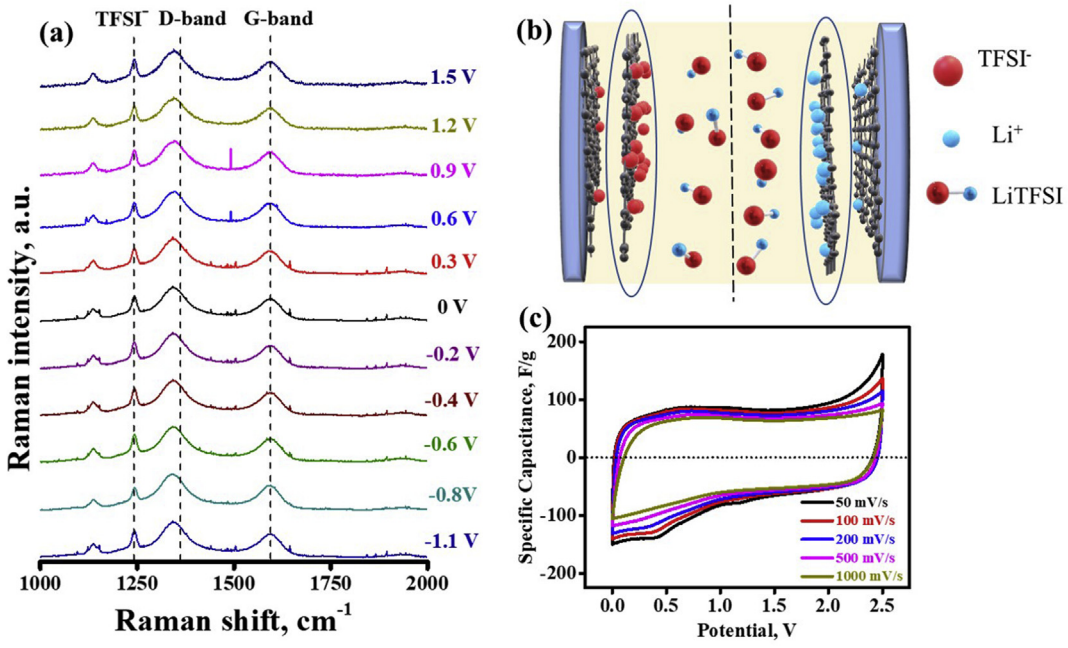

Fig. 2. Insitu Raman experiment at graphene SC electrodes: (a) LiTFSI anion and cation responses with respect to the applied potential (range from −1.1 V to 1.5 V) (b) Schematic illustration of surface adsorption of LiTFSI ions at Gr SC electrodes (c) Cyclic voltammetric response of Gr electrodes at different scan rates (range from 50 mV/s to 1000 mV/s).

surface area electrode material with limited/controlled pore size results in an enhanced rate capability. To further account this hypothesis, we carried out a CV experiment at different scan rates as shown in Fig. 2c. As expected, the shape of the CV curve remained rectangular even at a scan rate as high as 1000 mV/s (Fig. S5 c, d), indicating that higher rate capability can be achieved with WIS electrolytes. Fig. S7 represents log (scan rate) vs log (peak current) for the data obtained from CVs at different scan rates for both electrodes which represent charge storage mechanism, assuming that current obeys a power-law relationship, ($i = av^b$, where i is the measured current (mA), v is the scan rate (mV/s), a and b are the adjustable parameters). The slope of the plot, the value of b, close to 1 represents a surface or near-surface phenomenon indicating a capacitive charge storage mechanism, whereas a value close to 0.5 indicates a diffusion-controlled intercalation/deintercalation [46]. Obviously, graphene with a slope of 0.93 represents higher capacitive behavior due to faster ion adsorption or desorption on the surface, whereas, AC displayed value of 0.72 supporting the mechanism of diffusion of ions deep into its pores, thereby becoming inaccessible.

From the in situ Raman results, we evidenced that, WIS electrolyte ions undergo a surface dependent diffusional process at the interfaces. More specifically, on the surface having highly porous structures like AC, WIS electrolytes ions tend to enter into the pores which leads to a long range of ion transport pathways. Whereas, WIS ions undergo surface adsorption phenomenon on electrodes like Gr which facilitates a short range of ionic movements across the interface. As a result, EDLC charge storage mechanism and ion transport with WIS electrolytes directly are affected by the surface chemistry of carbon electrodes. Such SC electrode's surface dependent charge storage mechanisms and diffusion of ionic species are in good agreement with other concentrated electrolytes like ionic liquids [30,47].

To further corroborate the in situ Raman results, we performed alternating current (AC) based electrochemical impedance spectroscopy (EIS) as shown in Fig. 3. It is well known that EIS Nyquist and Bode plots can provide detailed information regarding the pore size dependent-accessibility of electrolyte ions and assist in elucidating the ion migration behavior at the interface, with respect to the applied frequencies. Fig. 3a represents the Nyquist plot, obtained in the frequency range of 1 MHz–100 mHz with a signal amplitude of 5 mV, for both activated carbon (AC) and modified graphene (Gr) based electrodes. The Nyquist plot reveals that the Gr electrode exhibits lower charge transfer resistance, as indicated by the absence of semicircle in the high-frequency region, whereas a pronounced semicircle was found in the case of AC electrodes. In the low-frequency region of the plot, Gr electrode exhibits nearly a vertical Warburg line (~80°) parallel to the imaginary axis, demonstrating typical capacitive behavior and high conductivity of the cell [48]. Whereas, Warburg line was found to be non-vertical in AC surface (~50°) and attributed to slower ion diffusion. The strong deviation of the Warburg component capacitive behavior from 90° in case of AC can be attributed to the broad pore size distribution of the electrodes, which enables the penetration of electrolyte ions deep into the pores [49].

Fig. 3b bode plot represents the real capacitance (C′, equation (1)) as a function of frequency which evaluates how many heavily solvated LiTFSI ions reach the porous carbon interface at a given

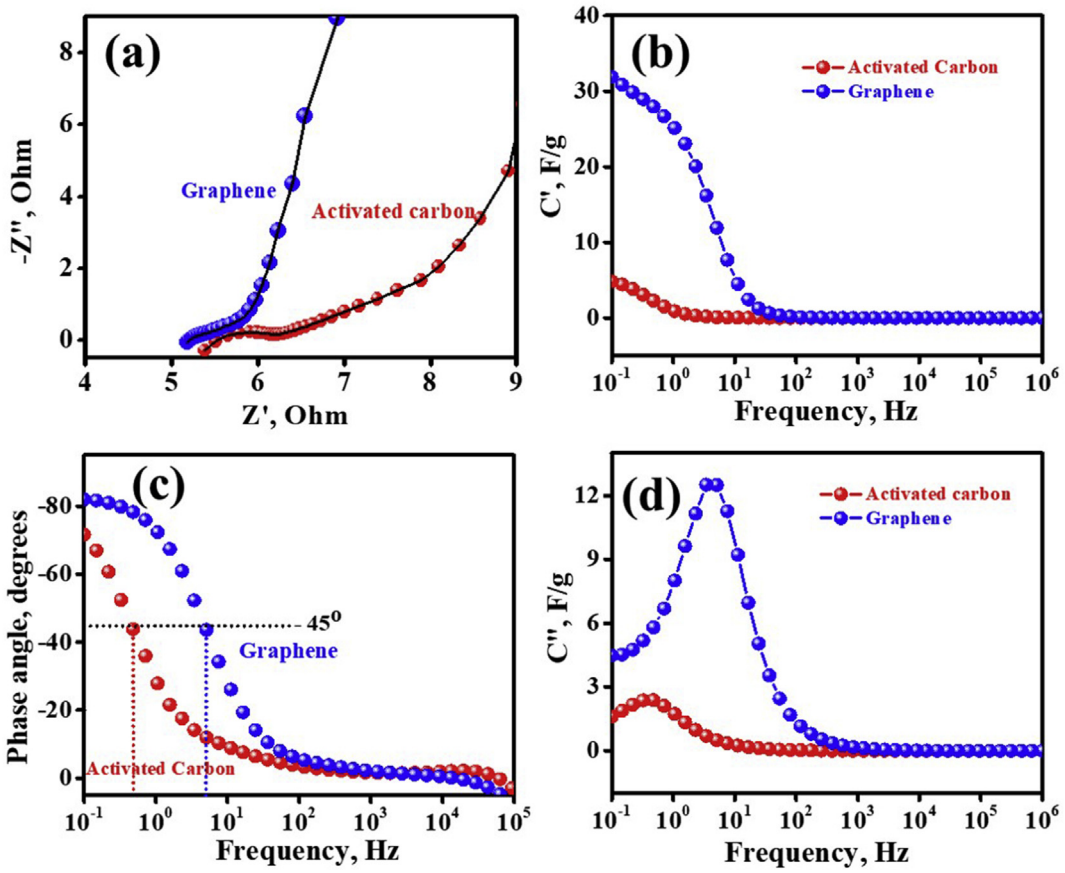

Fig. 3. Electrochemical impedance spectrography of activated carbon and graphene SC electrodes: (a) Nyquist plot; Bode plots of (b) Real capacitance as a function of frequency (c) phase angle plot (d) imaginary capacitance as a function of frequency. Frequency Range: 1 MHz–100mHz. Amplitude: 5 mV.

frequency region. Here, at low frequencies, the entire surface of the graphene electrode is accessible by the electrolyte ions, which results in the realization of a very large real capacitance. But, in the case of AC, the electrode's low surface area results in a decreased specific capacitance. With increasing frequency, C′ decreases and at frequencies above 100 Hz the real capacitance reached very low values. But, as can be clearly seen in Fig. 3b, C′ for Gr decreases at a slower rate than for AC, indicating an effective ion migration phenomenon on Gr. Also, at 1 Hz, the graphene electrode retained 80% of its maximum capacitance, which is 25 times more than that of AC, which further proves the importance of small ion pathways required to attain higher performance. This is further accounted by Bode plot of phase angle vs frequency (as shown in Fig. 3c) which demonstrates that at low-frequency region (<100 Hz) the phase shift was found to be −83° at 0.1 Hz on Gr electrodes which is more negative than AC (−72°). The decrease in phase angle for the AC electrodes indicates increased ion diffusion lengths and electrical resistance [50]. Furthermore, at a phase angle of −45° the characteristic frequency (f_o) known as knee frequency, which marks the point where the device behavior changes from purely resistive to capacitive [51], was found to be 5.64 Hz and 1.87 Hz for Gr and AC respectively. The knee frequency for Gr SC is at least 3 orders of magnitude higher than AC SC. It is a well-known fact that higher the knee frequency better is the rate capability, an important parameter that defines the performance of the SC. Fig. 3d presents a plot with imaginary capacitance (C″, given by equation (2)) as a function of frequency, which assists in the calculation of relaxation time constant (τ_o), a parameter which indicates the minimum time required to discharge the device's energy with an efficiency greater than 50% [34,52]. Time constants ($\tau_o = 1/2\pi f_o$, where f_o is the peak frequency) for Gr and AC SCs were 28 ms and 85 ms respectively, which indicates ultra-fast ion adsorption/desorption and an excellent rate capability at Gr electrodes over AC electrode. Thus, the outcome of EIS study along with detailed bode plot analysis demonstrates that carbon structure with morphology like Gr facilitates faster WIS ion migration compared to the porous structures like AC. It also confirms the dependency of capacitance and rate performance of SCs with WIS electrolytes purely upon the nature of electrodes and their pore size, while similar trends were observed with ionic liquids [30,47].

To prove the hypothesis that improvement of rate performance in WIS electrolytes is due to the surface area and pore size, we have performed typical galvanostatic charge-discharge experiments. As shown in Fig. S8, at a current density of 1 A/g, both devices exhibit a near triangular shaped charge-discharge curves. Since it is already established that, Gr has a uniform pore structure and high surface area, it is expected to show a higher capacitive behavior than AC. Fig. 4a shows the stable triangular charge-discharge curves of Gr SC even at scan rates as high as 10−50 A/g, which indicates an excellent capacitive nature with a high coulombic efficiency. The graphene electrodes showed capacitances (calculated according to equations (3) and (4)) of 345, 323, 277, 266, 216, 134 and 124 F/g at 0.5, 1, 2, 5, 10, 30 and 50 A/g current densities respectively. Such performance at current densities as high as 50 A/g is unparalleled with any of the latest reports in WIS electrolytes. In contrast, the values for AC were 50, 35, 29, 22 F/g at 0.5, 1, 2, 5 A/g respectively. The fast decay in the performance of AC can be ascribed to the increasing internal resistance with increasing current density. This is further corroborated by comparing rate performance at low current densities (Fig. 4b). The increase in the current density to a value as high as 50 A/g leads to a more pronounced specific capacitance decay in the Gr SC working cell, which can be attributed to the low ionic conductivity of WIS electrolytes. The specific capacitance retention at 50A/g was found to be 37% of the initial 0.5

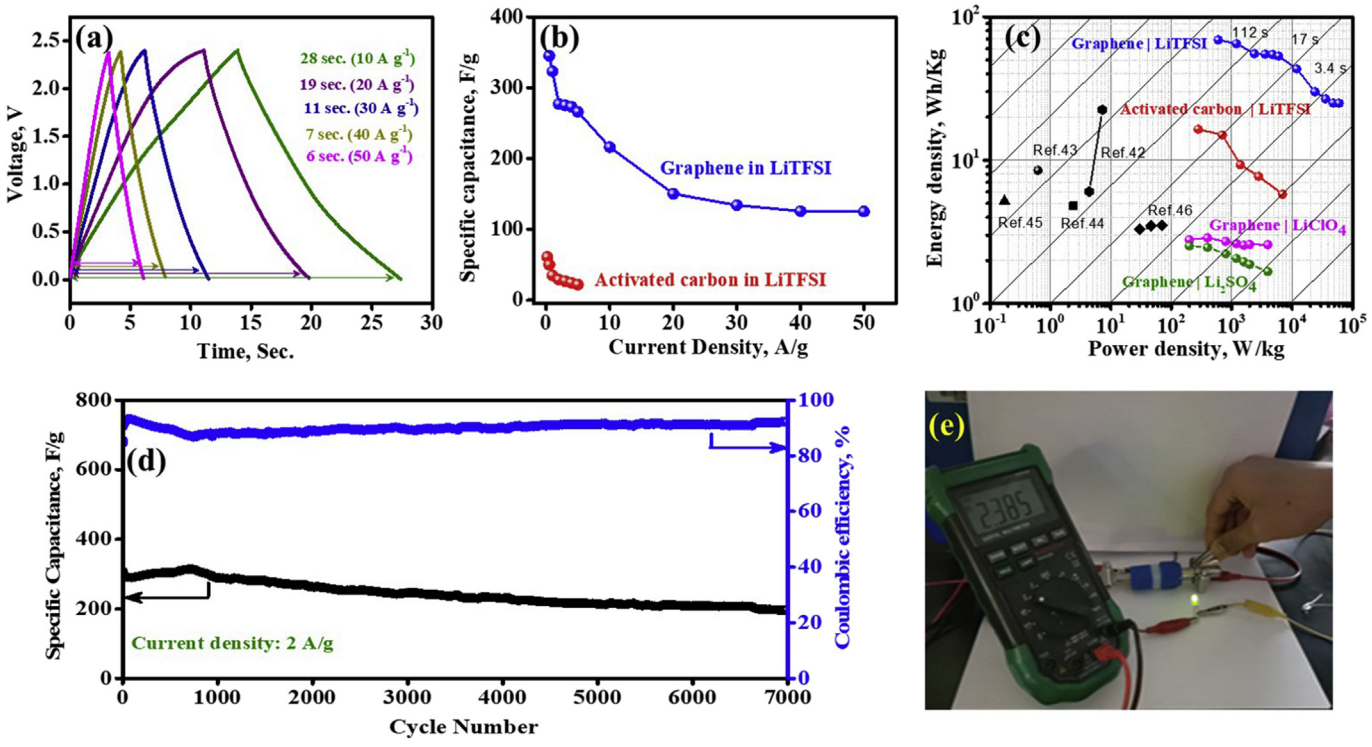

Fig. 4. Galvanostatic charge/discharge performance of graphene and activated carbon SC electrodes: (a) Voltage vs time response of Gr SC electrodes at high rate operation (from 10 A/g to 50 A/g) (b) Rate capability comparison of AC (red line) and Gr SC (blue line) electrodes (c) Power density vs Energy density (Ragone) comparison plot for Gr and AC electrodes in WIS, $LiClO_4$ and Li_2SO_4 electrolytes (d) SC long cycling performance of Gr electrode (e) LED powered by Gr supercapacitor. (For interpretation of the references to colour in this figure legend, the reader is referred to the Web version of this article.)

A/g current density, for the Gr-based cell whereas, the retention at a significantly lower current density of 5 A/g for the AC cell was found to be 35% from the initial 0.5 A/g. Thus, the drastic change in capacitance retention and high rate capability underlines the decisive role of electrode surface area and pore size nature in ensuring an efficient high-rate capacitive response. Table S1 (supporting information) shows the overall performance of both Gr and AC devices. With an identical cell setup, the specific capacitance of high-surface-area carbon, i.e. graphene in WIS electrolyte was found to be at least 7 times higher than that of the cell with AC electrodes.

Next, energy density and power density, crucial factors that decide the overall performance of a supercapacitor, were calculated according to equations (5) and (6). Fig. 4c shows the Ragone plot of the traditional salt-in-water electrolytes with Gr electrodes and water-in-salt electrolyte fabricated with AC and Gr electrodes. Conventional aqueous electrolytes in spite of having high ionic conductivity, suffer from an inherent low operating cell voltage. Hence this class of conventional salt-in-water electrolytes (e.g. Li_2SO_4), when operated between 0 V and 0.8 V, delivered a maximum energy density of 1.6 Wh/kg at a power density of 4 kW/kg. The reported energy and power density values for Gr electrodes in aqueous electrolytes, such as 6 M KOH, were 5.2 Wh/kg and 0.174 kW/kg respectively [53–58]. In the present work, AC SC delivered a maximum energy density of 5.8 Wh/kg at a power density of 7 kW/kg. On the other hand, Graphene cells with WIS electrolyte having an operating voltage of 0 V–2.4 V delivered a very high specific energy of 55.3 Wh/kg at a specific power of 2.4 kW/kg, which is about seven orders higher than activated carbon and several folds greater than the ones reported for traditional aqueous electrolytes with high surface area electrodes. The same Gr cell delivered an energy density of 43.3 Wh/kg at a power density of 12 kW/kg, which are almost comparable to that of hybrid graphene supercapacitors with ionic liquids reported recently, showing energy density of 44.7 Wh/kg at a power density of 4.5 kW/kg [59]. In short, the interfacial behavior of WIS electrolytes at porous electrodes is greatly affected by the surface area and pore size of the electrode. The availability of ions close to the surface due to the high surface area and pore size close to electrolyte ion size, alters the ion transportation process enhancing the capacitance which in turn leads to the realization of high specific energy.

Further, long-term cycling in AC SC electrodes, as shown in Fig. S9 reveals a drastic capacitance fade even within 1000 cycles, and the cell exhibited just over 70% capacitance retention. On the other hand, Fig. 4d shows a stable cycling behavior of Gr SC electrodes at 2 A/g, which exhibits a perfect triangular shape from the beginning of cycling until the end (Fig. S10). Even though a slight decrease in discharge time was noted after 5000 cycles, the cell exhibited over 93% capacitance retention over 7000 cycles, which demonstrates the high stability of SC with this electrolyte. As WIS electrolytes can undergo reduction they are often prone to the formation of solid products, when in the vicinity of the porous structure, they essentially clog the pores. Thus, the considerable deterioration of the AC electrodes visualized by the capacitance fade can be due to the lack of reversibility in exiting of ions from the AC porous structures. But, the excellent long cycling performance on Gr electrodes can be attributed to the surface adsorption mechanism of LiTFSI ions which cause minimal changes in the carbon structure. Fig. 4e shows a green 72 mW LED powered by a fully charged supercapacitor, indicating the promising usage of these devices for practical applications.

4. Conclusion

In conclusion, the change in interfacial dynamics of Water-in-salt electrolytes with respect to surface area and porous electrode were investigated in detail. In situ Raman experiments elucidate that WIS electrolyte ions undergo surface adsorption phenomena on Gr with a pore size of < 3 nm whereas diffusion of ions into the pores occurs at the highly porous AC structures (>30 nm). Further, electrochemical impedance results concluded that WIS electrolytes when used with Gr electrodes, reduces the ions diffusion pathway distances thereby assisting in the realization of extremely high real capacitances and rate performance. The obtained results suggest that ion storage at the Gr surface allows for quick sorption of ions with respect to the applied potential within a short span of time and enables the rapid charge/discharge process. This is further corroborated from the galvanostatic charge/discharge experiment which shows that carbon with a porous matrix like Gr delivers high rate performance as high as 50 A/g with 37% capacitance retention.

Notes

The authors declare no competing financial interest.

Acknowledgements

This article was supported in part by the National Science Foundation (Grant No. 1751472) and ACS Petroleum Research Fund (ACSPRF: 57647-DNI10). Authors would like to thank Dr. Kang Xu, United States Army Research Laboratory for providing the electrolytes for this study. This work made use of the JSM-7600 FE SEM supported by NSF Award#0922912. The authors would also like to thank Mr. Uday Praveen Tiruvalluri for designing the in situ electrochemical cell.

Appendix A. Supplementary data

Supplementary data to this article can be found online at https://doi.org/10.1016/j.electacta.2019.134989.

References

[1] P. Simon, Y. Gogotsi, Materials for electrochemical capacitors, Nat. Mater. 7 (2008) 845–854.
[2] C. Zhong, Y. Deng, W. Hu, J. Qiao, L. Zhang, J. Zhang, A review of electrolyte materials and compositions for electrochemical supercapacitors, Chem. Soc. Rev. 44 (2015) 7484–7539.
[3] L. Demarconnay, E. Raymundo-Piñero, F. Béguin, A symmetric carbon/carbon supercapacitor operating at 1.6V by using a neutral aqueous solution, Electrochem. Commun. 12 (2010) 1275–1278.
[4] Q. Gao, L. Demarconnay, E. Raymundo-Piñero, F. Béguin, Exploring the large voltage range of carbon/carbon supercapacitors in aqueous lithium sulfate electrolyte, Energy Environ. Sci. 5 (2012) 9611–9617.
[5] M. Bichat, E. Raymundo-Piñero, F. Béguin, High voltage supercapacitor built with seaweed carbons in neutral aqueous electrolyte, Carbon 48 (2010) 4351–4361.
[6] B.E. Conway, Electrochemical Supercapacitors: Scientific Fundamentals and Technological Applications, Springer Science & Business Media, 2013.
[7] M. Winter, R.J. Brodd, What are batteries, fuel cells, and supercapacitors? Chem. Rev. 104 (2004) 4245–4269.
[8] L.L. Zhang, X.S. Zhao, Carbon-based materials as supercapacitor electrodes, Chem. Soc. Rev. 38 (2009) 2520–2531.
[9] P. Liu, M. Verbrugge, S. Soukiazian, Influence of temperature and electrolyte on the performance of activated-carbon supercapacitors, J. Power Sources 156 (2006) 712–718.
[10] T. Tsuda, C.L. Hussey, Electrochemical applications of room-temperature ionic liquids, Interface-Electrochem. Soc. 16 (2007) 42–49.
[11] H. Liu, P. He, Z. Li, Y. Liu, J. Li, A novel nickel-based mixed rare-earth oxide/activated carbon supercapacitor using room temperature ionic liquid electrolyte, Electrochim. Acta 51 (2006) 1925–1931.
[12] K. Jurewicz, C. Vix-Guterl, E. Frackowiak, S. Saadallah, M. Reda, J. Parmentier, J. Patarin, F. Béguin, Capacitance properties of ordered porous carbon materials prepared by a templating procedure, J. Phys. Chem. Solids 65 (2004) 287–293.
[13] A. Pandolfo, A. Hollenkamp, Carbon properties and their role in supercapacitors, J. Power Sources 157 (2006) 11–27.
[14] F. Béguin, V. Presser, A. Balducci, E. Frackowiak, Carbons and electrolytes for

advanced supercapacitors, Adv. Mater. 26 (2014) 2219–2251.
[15] L. Suo, O. Borodin, T. Gao, M. Olguin, J. Ho, X. Fan, C. Luo, C. Wang, K. Xu, "Water-in-salt" electrolyte enables high-voltage aqueous lithium-ion chemistries, Science 350 (2015) 938–943.
[16] L. Suo, Y.S. Hu, H. Li, M. Armand, L. Chen, A new class of solvent-in-salt electrolyte for high-energy rechargeable metallic lithium batteries, Nat. Commun. 4 (2013) 1481.
[17] L. Suo, O. Borodin, W. Sun, X. Fan, C. Yang, F. Wang, T. Gao, Z. Ma, M. Schroeder, A. von Cresce, Advanced high-voltage aqueous lithium-ion battery enabled by "Water-in-Bisalt" electrolyte, Angew. Chem. Int. Ed. 55 (2016) 7136–7141.
[18] L. Suo, D. Oh, Y. Lin, Z. Zhuo, O. Borodin, T. Gao, F. Wang, A. Kushima, Z. Wang, H.-C. Kim, How solid-electrolyte interphase forms in aqueous electrolytes, J. Am. Chem. Soc. 139 (2017) 18670–18680.
[19] L. Suo, F. Han, X. Fan, H. Liu, K. Xu, C. Wang, "Water-in-Salt" electrolytes enable green and safe Li-ion batteries for large scale electric energy storage applications, J. Mater. Chem. 4 (2016) 6639–6644.
[20] R.S. Kuhnel, D. Reber, A. Remhof, R. Figi, D. Bleiner, C. Battaglia, "Water-in-salt" electrolytes enable the use of cost-effective aluminum current collectors for aqueous high-voltage batteries, Chem. Commun. 52 (2016) 10435–10438.
[21] P. Lannelongue, R. Bouchal, E. Mourad, C. Bodin, M. Olarte, S. le Vot, F. Favier, O. Fontaine, "Water-in-Salt" for supercapacitors: a compromise between voltage, power density, energy density and stability, J. Electrochem. Soc. 165 (2018) A657–A663.
[22] N. Kumar Thangavel, K. Mahankali, Y. Ding, L. Arava, Water-in-Salt Electrolytes for High-Voltage Supercapacitors, Meeting Abstracts, The Electrochemical Society, 2018, pp. 148–148.
[23] D. Reber, R.S. Kühnel, C. Battaglia, High-voltage aqueous supercapacitors based on NaTFSI, Sustainable. Energy. Fuels 1 (2017) 2155–2161.
[24] G. Hasegawa, K. Kanamori, T. Kiyomura, H. Kurata, T. Abe, K. Nakanishi, Hierarchically porous carbon monoliths comprising ordered mesoporous nanorod assemblies for high-voltage aqueous supercapacitors, Chem. Mater. 28 (2016) 3944–3950.
[25] G. Feng, S. Li, V. Presser, P.T. Cummings, Molecular insights into carbon supercapacitors based on room-temperature ionic liquids, J. Phys. Chem. Lett. 4 (2013) 3367–3376.
[26] J. Vatamanu, O. Borodin, Ramifications of water-in-salt interfacial structure at charged electrodes for electrolyte electrochemical stability, J. Phys. Chem. Lett. 8 (2017) 4362–4367.
[27] R. Burt, K. Breitsprecher, B. Daffos, P.L. Taberna, P. Simon, G. Birkett, X. Zhao, C. Holm, M. Salanne, Capacitance of nanoporous carbon-based supercapacitors is a trade-off between the concentration and the separability of the ions, J. Phys. Chem. Lett. 7 (2016) 4015–4021.
[28] D.E. Jiang, J. Wu, Microscopic insights into the electrochemical behavior of nonaqueous electrolytes in electric double-layer capacitors, J. Phys. Chem. Lett. 4 (2013) 1260–1267.
[29] F.W. Richey, B. Dyatkin, Y. Gogotsi, Y.A. Elabd, Ion dynamics in porous carbon electrodes in supercapacitors using in situ infrared spectroelectrochemistry, J. Am. Chem. Soc. 135 (2013) 12818–12826.
[30] F.W. Richey, C. Tran, V. Kalra, Y.A. Elabd, Ionic liquid dynamics in nanoporous carbon nanofibers in supercapacitors measured with in operando infrared spectroelectrochemistry, J. Phys. Chem. C 118 (2014) 21846–21855.
[31] J. Chmiola, G. Yushin, Y. Gogotsi, C. Portet, P. Simon, P.L. Taberna, Anomalous increase in carbon capacitance at pore sizes less than 1 nanometer, Science 313 (2006) 1760–1763.
[32] D. Pech, M. Brunet, H. Durou, P. Huang, V. Mochalin, Y. Gogotsi, P.L. Taberna, P. Simon, Ultrahigh-power micrometre-sized supercapacitors based on onion-like carbon, Nat. Nanotechnol. 5 (2010) 651.
[33] X. Sun, P. Cheng, H. Wang, H. Xu, L. Dang, Z. Liu, Z. Lei, Activation of graphene aerogel with phosphoric acid for enhanced electrocapacitive performance, Carbon 92 (2015) 1–10.
[34] P. Taberna, P. Simon, J.F. Fauvarque, Electrochemical characteristics and impedance spectroscopy studies of carbon-carbon supercapacitors, J. Electrochem. Soc. 150 (2003) A292–A300.
[35] B. Babu, M. Shaijumon, High performance sodium-ion hybrid capacitor based on Na2Ti2O4 (OH) 2 nanostructures, J. Power Sources 353 (2017) 85–94.
[36] A.L.M. Reddy, S. Ramaprabhu, Nanocrystalline metal oxides dispersed multiwalled carbon nanotubes as supercapacitor electrodes, J. Phys. Chem. C 111 (2007) 7727–7734.
[37] M.G. Hahm, A. Leela Mohana Reddy, D.P. Cole, M. Rivera, J.A. Vento, J. Nam, H.Y. Jung, Y.L. Kim, N.T. Narayanan, D.P. Hashim, C. Galande, Y.J. Jung, M. Bundy, S. Karna, P.M. Ajayan, R. Vajtai, Carbon nanotube–nanocup hybrid structures for high power supercapacitor applications, Nano Lett. 12 (2012) 5616–5621.
[38] L. Li, F. Sun, J. Gao, L. Wang, X. Pi, G. Zhao, Broadening the pore size of coal-based activated carbon via a washing-free chem-physical activation method for high-capacity dye adsorption, RSC Adv. 8 (2018) 14488–14499.
[39] Z. Song, H. Duan, D. Zhu, Y. Lv, W. Xiong, T. Cao, L. Li, M. Liu, L. Gan, Ternary-doped carbon electrodes for advanced aqueous solid-state supercapacitors based on a" water-in-salt" gel electrolyte, J. Mater. Chem. 7 (2019) 15801–15811.
[40] Z. Song, H. Duan, L. Li, D. Zhu, T. Cao, Y. Lv, W. Xiong, Z. Wang, M. Liu, L. Gan, High-energy flexible solid-state supercapacitors based on O, N, S-tridoped carbon electrodes and a 3.5 V gel-type electrolyte, Chem. Eng. J. 372 (2019) 1216–1225.
[41] J. Yan, D. Zhu, Y. Lv, W. Xiong, M. Liu, L. Gan, Water-in-salt electrolyte ion-matched N/O codoped porous carbons for high-performance supercapacitors, Chin. Chem. Lett. (2019), https://doi.org/10.1016/j.cclet.2019.05.035.
[42] L. Suo, F. Zheng, Y.S. Hu, L. Chen, FT-Raman spectroscopy study of solvent-in-salt electrolytes, Chin. Phys. B 25 (2015), 016101.
[43] G. Dresselhaus, R. Saito, G. Dresselhaus, Raman Spectroscopy in Graphene Related Systems, Wiley-VCH, Europe, 2011.
[44] A.C. Ferrari, J. Meyer, V. Scardaci, C. Casiraghi, M. Lazzeri, F. Mauri, S. Piscanec, D. Jiang, K. Novoselov, S. Roth, Raman spectrum of graphene and graphene layers, Phys. Rev. Lett. 97 (2006) 187401.
[45] E. Redondo, E. Goikolea, R. Mysyk, The decisive role of electrolyte concentration in the performance of aqueous chloride-based carbon/carbon supercapacitors with extended voltage window, Electrochim. Acta 221 (2016) 177–183.
[46] X. Xiao, H. Song, S. Lin, Y. Zhou, X. Zhan, Z. Hu, Q. Zhang, J. Sun, B. Yang, T. Li, Scalable salt-templated synthesis of two-dimensional transition metal oxides, Nat. Commun. 7 (2016) 11296.
[47] F.W. Richey, B. Dyatkin, Y. Gogotsi, Y.A. Elabd, Ion dynamics in porous carbon electrodes in supercapacitors using in situ infrared spectroelectrochemistry, J. Am. Chem. Soc. 135 (2013) 12818–12826.
[48] K. Sheng, Y. Sun, C. Li, W. Yuan, G. Shi, Ultrahigh-rate supercapacitors based on electrochemically reduced graphene oxide for ac line-filtering, Sci. Rep. 2 (2012) 247.
[49] M. Toupin, D. Bélanger, I.R. Hill, D. Quinn, Performance of experimental carbon blacks in aqueous supercapacitors, J. Power Sources 140 (2005) 203–210.
[50] J. Lin, C. Zhang, Z. Yan, Y. Zhu, Z. Peng, R.H. Hauge, D. Natelson, J.M. Tour, 3-dimensional graphene carbon nanotube carpet-based microsupercapacitors with high electrochemical performance, Nano Lett. 13 (2012) 72–78.
[51] W. Zhe, S. Yang, W. Da-Wei, L. Feng, D. Jinhong, C. Hui-Ming, Graphene–cellulose paper flexible supercapacitors, Adv. Energy. Mater. 1 (2011) 917–922.
[52] B. Fang, L. Binder, A novel carbon electrode material for highly improved EDLC performance, J. Phys. Chem. B 110 (2006) 7877–7882.
[53] F. Markoulidis, C. Lei, C. Lekakou, D. Duff, S. Khalil, B. Martorana, I. Cannavaro, A method to increase the energy density of supercapacitor cells by the addition of multiwall carbon nanotubes into activated carbon electrodes, Carbon 68 (2014) 58–66.
[54] Q. Shao, J. Tang, Y. Lin, J. Li, F. Qin, J. Yuan, L.C. Qin, Carbon nanotube spaced graphene aerogels with enhanced capacitance in aqueous and ionic liquid electrolytes, J. Power Sources 278 (2015) 751–759.
[55] X. Li, W. Xing, S. Zhuo, J. Zhou, F. Li, S.Z. Qiao, G.Q. Lu, Preparation of capacitor's electrode from sunflower seed shell, Bioresour. Technol. 102 (2011) 1118–1123.
[56] Z. Lei, Z. Liu, H. Wang, X. Sun, L. Lu, X.S. Zhao, A high-energy-density supercapacitor with graphene-CMK-5 as the electrode and ionic liquid as the electrolyte, J. Mater. Chem. 1 (2013) 2313–2321.
[57] P. Chen, J.J. Yang, S.-S. Li, Z. Wang, T.Y. Xiao, Y.H. Qian, S.H. Yu, Hydrothermal synthesis of macroscopic nitrogen-doped graphene hydrogels for ultrafast supercapacitor, Nano Energy 2 (2013) 249–256.
[58] D. Jiménez-Cordero, F. Heras, M.A. Gilarranz, E. Raymundo-Piñero, Grape seed carbons for studying the influence of texture on supercapacitor behaviour in aqueous electrolytes, Carbon 71 (2014) 127–138.
[59] N. Ma, N. Phattharasupakun, J. Wutthiprom, C. Tanggarnjanavalukul, P. Wuanprakhon, P. Kidkhunthod, M. Sawangphruk, High-performance hybrid supercapacitor of mixed-valence manganese oxide/N-doped graphene aerogel nanoflower using an ionic liquid with a redox additive as the electrolyte: in situ electrochemical X-ray absorption spectroscopy, Electrochim. Acta 271 (2018) 110–119.